Research paper

A Bayesian surrogate constitutive model to estimate failure probability of elastomers

Aref Ghaderi [a], Vahid Morovati [b], Roozbeh Dargazany [a],*

[a] *Department of Civil and Environmental Engineering, Michigan State University, United States of America*
[b] *Department of Aerospace Engineering and Engineering Mechanics, University of Texas at Austin, United States of America*

A B S T R A C T

To calculate the uncertainty in the failure probability of elastomeric materials, a parametric and a non-parametric Bayesian-based stochastic constitutive model were evaluated. (i) A Bayesian linear regression calibration technique is created based on the Carroll model to construct a probabilistic hyper-elastic model in the parametric approach. The model was then calibrated using two methods: Maximum Likelihood Estimation (MLE) and Maximum a Posteriori (MAP) estimation, with the results compared. (ii) The Gaussian process (GP) is used in non-parametric hyper-parameters of the radial basis kernel computed using the limited-memory Broyden–Fletcher–Goldfarb–Shanno technique. Both models were trained and verified with regard to two sets of our experiments on silicon- and polyurethane-based elastomers to demonstrate their capabilities in modeling uncertainty propagation. Finally, failure probability analysis was carried out for these data sets using First Order Reliability Method (FORM) analysis and Crude Monte Carlo (CMC) simulation, with a limit state function based on the stochastic constitutive model at the failure point. Sensitivity analysis is also used to demonstrate the importance of Carroll model parameters in predicting failure likelihood. The results show that the parametric approach has great agreement with experimental data, not only for uncertainty quantification and model calibration, but also for calculating the failure probability of hyperelastic materials.

1. Introduction

In many applications, proper prediction of the end-life of rubber-like materials has been a subject of significant interest, which comes with major challenges. One major challenge is the large uncertainty observed in the behavior of elastomers induced by intrinsic defects, processing, sample manufacturing, or simply heterogeneous nature of the matrix. Elastomers are often made by highly cross-linked polymer matrix that behave fully elastic with entropic force, which results in a highly non-linear behavior, especially during large deformation and significant hardening observed before failure.

The hyperelastic behavior of isotropic incompressible rubbers has been studied to establish a function of strain energy that meets all the physical and continuum conditions (Mooney, 1940; Ogden, 1972; Arruda and Boyce, 1993). The development of constitutive models for rubber-like materials is hindered by both incompleteness of the theoretical approach and limitation in experiment observation.

In the past decades, researchers have proposed many deterministic constitutive models based on materials' average response to mechanical elongation without considering uncertainty (Steinmann et al., 2012;

Liao et al., 2020, 2021). Thus, it was challenging to calculate confidence bounds in prediction of the material response or reduce the error of the model. In addition, one of the main challenges in deterministic approaches is the intrinsic variation of failure stretch/stress of different samples, which cannot be described by deterministic methods. So, state of failure can be better defined as a Fuzzy variable rather than a binary process which is the main focus of this study.

The study of quantitative characterization and the elimination of uncertainties in both computational and real-world applications is known as uncertainty quantification (UQ). If certain elements of a system are not exactly understood, UQ try to quantify how relevant those elements are. UQ can limit the range of validity of the model predictions by providing the error bounds. Most current models are developed based on a deterministic approach, where a specific and certain response is calculated to describe the average response of the system. However, in real-life applications, the behavior of the polymeric systems mostly follow a probabilistic pattern, which limits the relevance of deterministic models (Honarmandi, 2019; Cao et al., 2021). One major advantage of UQ is that the probabilistic models can provide multiple sets of values for material parameters to fit certain behavior in the form of

---

* Corresponding author.
E-mail addresses: ghaderi1@msu.edu (A. Ghaderi), morovati@austin.utexas.edu (V. Morovati), roozbeh@msu.edu (R. Dargazany).

the probability distribution of model prediction through uncertainty propagation. Such variation of the parameters allows users to study and predict system behavior in unexpected events, in particular in failure prediction. In deterministic models, failure is described to occur abruptly and surely once the nominal stress σ exceeds a deterministic failure strength threshold σ_f. However, in a probabilistic approach, both σ and σ_f are defined as probabilities, and thus with an increase of stress, only the probability of failure increases without providing a particular location for failure.

So, considering the occurrence of the failure as a probabilistic parameter rather than a black or white event, one can classify the observed uncertainty as the superposition of two different errors, namely (i) "epistemic errors" are often induced by lack of knowledge and can be reduced by assigning additional resources, and (ii) "aleatory errors" are intrinsic error of the system, which cannot be reduced and can only be shifted from one parameter to another. The goal of UQ in computational modeling is the calculation of uncertainty in the modeling and its prediction (Yang et al., 2019; Pouresmaeeli et al., 2018). Two statistical views usually evaluate the quantification process: the frequentist view, which defines probability during a long-term observation based on the rate of occurrence, and the Bayesian view, which considers the degree of belief based on the combination of prior knowledge and new data for probability. So, in the frequentist view, parameters are *fixed random variables*. However, in the Bayesian perspective, parameters are *random variables based on the available data*. Although incorrect prior knowledge can mislead the model, the true definition is helpful in statistical inference (Rocchetta et al., 2018; Ghanipour et al., 2018). So, uncertainty quantification is the prerequisite of the calculation of failure probability.

Several deterministic models have been proposed during past decades. In 1948, Rivlin (1948) investigated fundamental concepts of large elastic deformation of isotropic materials. In 2020, we proposed a physics-based data-driven constitutive model for cross-linked polymers by embedding neural networks in micro-sphere (Ghaderi et al., 2020).

In recent years, several studies have been conducted on the stochastic modeling of constitutive models of soft materials (Madireddy et al., 2015; Brewick and Teferra, 2018; Fitt et al., 2019). In 2015, a Bayesian parametric approach was employed for calibration of the constitutive model for soft tissue based on Bayes factors (Madireddy et al., 2015). Brewick and Teferra (2018) derived a parametric UQ model of Ogden model for brain tissue. They calculated posterior distribution of the constitutive parameters by employing Markov Chain Monte Carlo. Kamiński and Lauke (2018), derived parametric UQ models of multiple constitutive models ranging from Neo-Hookean to Arruda–Boyce, and showed probabilistic characteristics, such as expectation, variance, skewness, and kurtosis.Recently, Fitt et al. (2019) published their study on the uncertainty quantification of elastic materials by using Bayes' theorem to select the model. Another parametric study has been used as a Bayesian calibration framework to determine the posterior parameter distributions of a hyper-viscoelastic constitutive model using mechanical testing data of brain tissue (Teferra and Brewick, 2019).

While several studies were conducted on predicting the failure probability of materials and structures, Orta and Bartlett (2015), Dimitrov et al. (2017), Mishra et al. (2019) and Khashaba et al. (2017) the failure of rubber-like materials remains a challenging issue. Here, our goal is to advance a parametric UQ approach to predict failure probability from the Carroll constitutive model. The model is then compared with predictions of a non-parametric UQ approach which comes at considerably higher computational cost. Note that we selected the Carroll model because compared to other complex model such as microsphere model and tube model it is simpler with equal accuracy for both Treloar's and Kawataba's dataset (Dal et al., 2021). Carroll model not only has just three parameters but also it can capture the behavior of elastomers in different states of deformation such as biaxial, and

shear because it is function of first and second invariants of deformation tensor.

In this contribution, our goal is to carry out three fundamental steps in probabilistic modeling of elastomers, namely (i) Bayesian evaluation of constitutive model (Carroll model Carroll, 2011) parameters for hyperelastic behavior of rubber-like materials from two distinct experimental data, (ii) Development of confidence bounds for stress–strain curves based on conjugate prior, and (iii) failure probability was calculated based on First Order Reliability Method (FORM) and validated against that of Crude Monte Carlo (CMC) simulation to provide a sensitivity analysis on the effect of model parameters on failure probability.

This work presents two stochastic models as prerequisite of calculation of failure probability. The proposed method can be presented in the following steps:

Step 1 Proposing a Bayesian-based **parametric** stochastic model *for smooth data* built on the Carroll model (Carroll, 2011), which is developed using Bayesian statistics calibration

Step 2 proposing a **non-parametric** stochastic constitutive model *for noisy data* based on Gaussian Process (GP).

Step 3 By training both models by constitutive behavior of silicon- and polyurethane-based adhesives, we show that both approaches can provide accurate predictions in rubber-like materials.

Step 4 We will develop a probabilistic failure model based on the parametric stochastic model using the limit state function, which can also be developed using the same approach for non-parametric constitutive models, although with higher computational cost and a different implementation strategy.

Step 5 Predicting the failure using FORM method, a sensitivity analysis is employed to show the importance of each parameter of constitutive model in the probability of failure, and validate the predictions against those of CMC method.

The rest of this manuscript is organized as follows. In Section 2, a parametric stochastic constitutive model based on Bayesian model calibration is mentioned for both cases of maximum prior estimation and maximum likelihood estimation. Next, we discuss GP as a non-parametric model in detail for finding hyper-parameters of the kernel-based on the limited-memory Broyden–Fletcher–Goldfarb–Shanno (L-BFGS) method in Section 3. Moreover, the probability of failure analysis based on FORM and CMC simulations are explained in Section 4. Finally, the results are presented in Section 5 for two compounds tested in our facility as are described in details.

2. Parametric approach

The first step in parametric calculation of the failure probability is making a stochastic surrogate model from the behavior of materials. To this end, a probabilistic constitutive model is required to model uncertainties which affect the materials' behavior.

In UQ analysis, one way to categorize the sources of uncertainty is to consider: (1) *Parameter uncertainty* which comes from the model parameters that are inputs to the computer model (mathematical model) but whose exact values are unknown to experimentalists and cannot be controlled in physical experiments, or whose values cannot be exactly inferred by statistical methods. (2) *Structural uncertainty* known as model inadequacy, model bias, or model discrepancy, this comes from the lack of knowledge of the underlying physics in the problem. (3) *Algorithmic uncertainty* known as numerical uncertainty, or discrete uncertainty. This type comes from numerical errors and numerical approximations per implementation of the computer model. (4) *Experimental uncertainty* known as observation error, this comes from the variability of experimental measurements. (5) *Interpolation uncertainty* which comes from a lack of available data collected from computer model simulations and/or experimental measurements.

In the Parametric Stochastic Constitutive model, the hyper-elastic response is characterized by Carroll model (Carroll, 2011). The strain

energy function Ψ and uni-axial stress of the Carroll model P^{UT} are given as

$$\Psi = W_1 I_1 + W_2 I_1^4 + W_3 \sqrt{I_2}, \tag{1}$$

$$P^{UT} = \left(2W_1 + 8W_2 \left(2\lambda^{-1} + \lambda^2 \right)^3 + W_3 \left(1 + 2\lambda^3 \right)^{-\frac{1}{2}} \right) \left(\lambda - \lambda^{-2} \right), \tag{2}$$

where λ is the principal stretch in the uni-axial tensile loading, I_1 and I_2 are the second invariant of Green–Cauchy tensor (Appendix), and $W_i |_{i=1..3}$ are model parameters.

Let us first describe the steps required for the calibration of a constitutive model as a stochastic model. A constitutive model should be able to connect deformation input λ to stress output P through certain internal parameters W such that

$$P = f(\lambda; W) + \epsilon, \quad with \quad f(\lambda; W) = \sum_{j=1}^{m} W_j \phi_j(\lambda), \quad and$$

$$\mathcal{P}(\epsilon) = N \left(\epsilon | 0, \sigma^2 \right), \tag{3}$$

where ϕ_j are the basis functions, m is the number of basis functions, and W_j are the weight parameters gathered in vector W. Here, $N \left(\epsilon | 0, \sigma^2 \right)$ represents the Gaussian distribution of noise around zero with variance σ^2 which is assumed to represent $\mathcal{P}(\epsilon)$. Inserting Carroll model (Carroll, 2011) in Eq. (2), $f(\lambda; W) D$ will be represented by three weight parameters and three basis functions, where $m = 3$. As a representative constitutive models, the Carroll model (Carroll, 2011) is chosen due to its performance in predicting different states of deformation, which has a rational error. In a stochastic calibration problem (Mihai et al., 2018), we optimize function $f(\lambda; W)$ by fitting W with a dataset D of n observations of λ, and P as summarized below

$$D = \left\{ \left[\lambda_1, P_1 \right] \dots \left[\lambda_n, P_n \right] \right\} = \{ P, \lambda \}. \tag{4}$$

Bayesian Methodology is used to calculate the joint probability distribution of model parameters and accordingly to derive uncertainty associated with experimental data (Box and Tiao, 2011). In comparison to the least square method (LSM), the Bayesian approach can show the model uncertainty with stochastic parameters, while LSM mainly search for the best parameters for fitting without providing any information regarding parameters' probability. Bayesian method is based on the Bayes conditional rule of probability where

$$\mathcal{P}(W|D, M) = \frac{\mathcal{P}(D|W, M) \mathcal{P}(W|M)}{\mathcal{P}(D)}, \tag{5}$$

which W is the vector of unknown model parameters, and M is the chosen model, namely, the Carroll model (Carroll, 2011). $\mathcal{P}(W|M)$ is the prior joint distribution and shows the degree of belief to the parameters before we know the data. $\mathcal{P}(D|W, M)$ is the likelihood joint distribution which describes the observation probability of what we have observed, and $\mathcal{P}(W|D, M)$ is the posterior distribution. Here, $\mathcal{P}(D)$ is a normalizer, given as follow

$$\mathcal{P}(D) = \int_W \mathcal{P}(D|W, M) \mathcal{P}(W|M) dW. \tag{6}$$

For parameter estimation, the marginal likelihood $\mathcal{P}(D)$ does not affect the value of the weight parameters W, so it is often considered as a normalization constant. In the absence of any information, the prior probability of the parameters can be assumed to be a Gaussian distribution on the parameter space. It is one way to illustrate our prior ignorance about the weight parameters W.

Selection of prior is an important step in Bayesian approach, which can be accomplished using different approaches such as right Haar measurement, Jeffreys prior (Robert, 2007), reference priors (Berger and Bernardo, 1992), Maxent priors (Jaynes, 2003), conjugate priors (Vila et al., 2000). Conjugate priors, unlike other methods, lead to the specific family of distributions for posterior distributions. In this study, we choose prior from the Gaussian family to make the integration of Bayes rule simpler compared to other methods that are problematic and not

practical for feeding failure probability analysis. This selection does not affect results significantly because new observation leads to updating of prior distribution after each step. Meanwhile, model selection strategies are manyfold in Bayesian methodology. Bayesian methods using Bayes factor, frequentist methods, and Bayesian Information Criterion are the most popular approaches. The Bayesian method has certain benefits over the strategies of frequentism. First, the model's posterior probabilities and the Bayes factor are easier to understand as the odds of one model over the other. Second, the Bayesian method is compatible in the sense that if it is part of the candidate model set under very mild conditions, it ensures the choice of the true model (Berger et al., 2001; Berk, 1966). Accordingly, our Prior can be given as

$$\mathcal{P}(W; \alpha) = \mathcal{N} \left(W | 0, \frac{1}{\alpha} I \right), \tag{7}$$

where the initial assumption is to distribute the weights around zero, $\mathcal{N}\left(W | 0, \alpha^{-1} I \right)$, with precision parameter α(Tipping, 2001; Chen and Martin, 2009) for MAP that serves as a regulatory index to prevent overfitting and with precision parameter α equal to 1 for MLE. The precision parameter is associated with the uncertainty over values of W.

Model Calibration will be carried out using two different methods to validate them against each other, (i) Maximum Likelihood Estimation (MLE), and (ii)Maximum a Posterior (MAP) estimation are Burr (2004).

2.1. Maximum Likelihood Estimation (MLE)

The concept of MLE seeks a probability distribution that "most likely" regenerate the observations. In other words, it seeks a weight parameter vector, W_{MLE} which maximizes the likelihood function $\mathcal{P}(W|D, M)$. MLE estimates, W_{MLE}, may not exist nor be unique. To reduce computational costs, W_{MLE} is often obtained by maximizing the log of the likelihood function, $\ln \mathcal{P}(W|D, M)$, which has a significantly slower growth rate. In essence, since both the likelihood function and its log function are monotonically related to each other, W_{MLE} should maximize both. Assuming log-likelihood to be differentiable, MLE principal yields the following conditions

$$\left. \frac{\partial \ln \mathcal{P}(W|D, M)}{\partial W} \right|_{W = W_{MLE}} = 0, \qquad \left. \frac{\partial^2 \ln \mathcal{P}(W|D, M)}{\partial W^2} \right|_{W = W_{MLE}} < 0, \tag{8}$$

where the second condition ensures the convexity of the function at the optimum W_{MLE}. Rewriting Eq. (5) with respect to stress and deformation, the posterior summarizes our state of knowledge after observing constitutive data if we know the noise variance σ^2. In view of Eq. (5), the posterior is given as

$$\mathcal{P}\left(W | \lambda, P; \sigma^2 \right) = \frac{\mathcal{P}\left(P | \lambda, W; \sigma^2 \right) \mathcal{P}(W)}{\mathcal{P}(P | \lambda)},$$

$$\mathcal{P}(P | \lambda) = \int \mathcal{P}\left(P | \lambda, W; \sigma^2 \right) \mathcal{P}(W) dW, \tag{9}$$

where $\mathcal{P}(P | \lambda)$ is the marginal likelihood of producing the experimental dataset D. Assuming likelihood and prior to be Gaussian, we can write the likelihood function with respect to Eq. (8) as

$$\mathcal{P}\left(P | \lambda, W; \sigma^2 \right) = \exp \left(-\frac{1}{2\sigma^2} \| \Phi W - P \|^2 \right) \tag{10}$$

where $\Phi \in \mathbb{R}^{n \times m}$ is a matrix with values of basis functions distributed over observation points D such that $\Phi_{i,j} = \phi_i(\lambda_j)$. In MLE approach, one can find the weight parameters, W_{MLE}, by derivation from Eq. (10)

$$\nabla \mathcal{P}\left(P | \lambda, W; \sigma^2 \right) = 0 \quad \Rightarrow \quad W_{MLE} = \left(\Phi^T \Phi \right)^{-1} \Phi^T P,$$

$$\sigma_{MLE}^2 = \frac{\| \Phi W_{MLE} - P \|^2}{n}. \tag{11}$$

The posterior function is consequently derived as a PDF function of multivariate distribution $\mathcal{N}$ as

$$\mathcal{P}\left(\boldsymbol{P}|\lambda, \boldsymbol{W}; \sigma^2\right) = \mathcal{N}\left(\boldsymbol{P}|\boldsymbol{W}_{MLE}^T \boldsymbol{\Phi}(\lambda); \sigma_{MLE}^2\right). \tag{12}$$

The posterior function allows us to make a probability distribution for a new target constitutive values λ^*, and σ^* based on the optimized weight parameters $\boldsymbol{W}_{MLE}$ using $\mathcal{P}(\boldsymbol{P}^*|\lambda^*, \boldsymbol{W}_{MLE}; \sigma)$, where the median $m(\lambda)$, lower bound $l(\lambda)$, and upper bound $u(\lambda)$, for any new target deformation can be calculated as

$$m(\lambda) = \sum_{j=1}^{m} W_{MLE:j} \phi_j(\lambda), \qquad l(\lambda) \approx m(\lambda) - 2\sigma_{MLE},$$

$$u(\lambda) \approx m(\lambda) + 2\sigma_{MLE}. \tag{13}$$

2.2. Maximum a posteriori (MAP) estimation

In this method, the measurement process is modeled using the posterior to find parameters. We believe that our measurement is around the model prediction, but it is contaminated by Gaussian noise. So, we have the same likelihood here Eq. (10). The difference between this method with the last method is, here, we maximize posterior. This method is very similar to MLE, with the addition of the prior probability over the distribution and parameters. In fact, if we assume that all values of weights are equally likely because we do not have any prior information, then both calculations are equivalent. Thus, both MLE and MAP often converge to the same optimization problem for many machine learning algorithms because of this equivalence. This is not always the case. If the calculation of the MLE and MAP optimization problem differ, the MLE and MAP solution found for an algorithm may also differ. We model the uncertainty in model parameters using a prior. In the MAP approach, the likelihood function in Eq. (9) will be calculated differently based on conjugate prior and given as

$$\mathcal{P}(\boldsymbol{P}|\lambda, \boldsymbol{W}; \sigma) = \exp\left(-\frac{1}{2\sigma^2}\|\boldsymbol{\Phi}\boldsymbol{W} - \boldsymbol{P}\|^2 - \frac{\alpha}{2}\|\boldsymbol{W}\|^2\right), \tag{14}$$

where one can find the optimized weight parameters that are gathered in $\boldsymbol{W}_{MAP}$, by derivation from Eq. (14)

$$\nabla \mathcal{P}\left(\boldsymbol{P}|\lambda, \boldsymbol{W}; \sigma^2\right) = 0 \quad \Rightarrow \quad \boldsymbol{W}_{MAP} = \arg\max \log \mathcal{P}\left(\boldsymbol{P}|\lambda, \boldsymbol{W}; \sigma\right)$$

$$= \mathbf{S}_M \boldsymbol{\Phi}^T \boldsymbol{P}, \qquad \mathbf{S}_M = \left(\alpha \mathbf{I} + \frac{1}{\sigma^2}\boldsymbol{\Phi}^T \boldsymbol{\Phi}\right)^{-1}. \tag{15}$$

The posterior function is consequently derived as

$$\mathcal{P}(\boldsymbol{W}|\lambda, \boldsymbol{P}) = \mathcal{N}\left(\boldsymbol{W}|\boldsymbol{W}_N, \mathbf{S}_N\right) = \det\left(2\pi \mathbf{S}_N\right)^{-\frac{1}{2}}$$

$$\times \exp\left(-\frac{1}{2}(\boldsymbol{W} - \boldsymbol{W}_N)^T \mathbf{S}_N^{-1}(\boldsymbol{W} - \boldsymbol{W}_N)\right), \tag{16}$$

where $\boldsymbol{W}_N$ is the mean vector, $\mathbf{S}_N$ is covariance matrix, and for a Gaussian posterior, $\boldsymbol{W}_{MAP} = \boldsymbol{W}_N$, and $\mathbf{S}_M = \mathbf{S}_N$. The posterior function allows us to make a probability distribution for a new target deformation values λ^* based on the optimized weight parameters $\boldsymbol{W}_{MAP}$ as

$$\mathcal{P}\left(\boldsymbol{P}^*|\lambda^*, \boldsymbol{W}_N, \mathbf{S}_N\right) = \mathcal{N}\left(\boldsymbol{P}^*|\boldsymbol{W}_N^T \phi(\lambda^*), \mathbf{S}_N\right), \tag{17}$$

where the median $m(\lambda)$, lower bound $l(\lambda)$, and upper bound $u(\lambda)$, for any new target deformation can be calculated as

$$m(\lambda) = \sum_{j=1}^{m} W_{MAP:j} \phi_j(\lambda), \qquad l(\lambda) \approx m(\lambda) - 2\sigma, \qquad u(\lambda) \approx m(\lambda) + 2\sigma. \tag{18}$$

3. Non-parametric approach

A Non-parametric Stochastic Constitutive Model is proposed to describe the constitutive behavior of elastomers and its associated uncertainty. Unlike parametric method, this method is generic and can

be applied to any mapping ranging simple to complex, although at significantly higher computational cost (Planas et al., 2021; Bostanabad et al., 2020). Gaussian processes (GP) take a non-parametric approach to model selection. Compared to Bayesian linear regression, GP is more general because the form of the classifier is not limited by a parametric form (Fuhg et al., 2021a,b). GP can also handle the case in which data is available in different forms, as long as we can define an appropriate covariance function for each data type. Bessa et al. (2017) and Liu et al. (2016) employed Gaussian processes and neural networks to create a constitutive model for hyperelastic materials, and also to predict plastic properties.

Gaussian process (GP). represents the probability of function outputs by providing a joint Gaussian distribution of the output for any set of input points (Rasmussen, 2003). This property, and the fact that the distribution of a subset conditioned on the rest is also Gaussian for any set of observations with a joint Gaussian distribution, allows predictions to be made at an unknown point (λ^*) based on previous observations $\boldsymbol{D}$. A GP on a model can be written as

$$\mathcal{P}(\boldsymbol{P}) = \mathcal{G}_{\mathcal{P}}\left\{\boldsymbol{P}|\mu; \mathbf{K}(\lambda, \lambda)\right\} \tag{19}$$

where μ is the mean function which indicates the central tendency of the $\mathcal{G}_{\mathcal{P}}$. Assuming no particular knowledge about the trend of the function, we pick a zero mean function. $\mathcal{P}(\boldsymbol{P})$ denotes our beliefs about $\boldsymbol{P}$. Tensor $\mathbf{K}$ is symmetric matrix (kernel) that describes the covariance between every pair of components in the input vector λ and depends on a set of hyperparameters θ. There is a one-to-one correspondence between the differentiability of the covariance function and samples from the GP probability measurement of the GP probability measurement when selecting the covariance function model (Adler, 2010). Describing $\mathbf{K}$ using the squared exponential covariance function, we can write the components as

$$K_{ij} = k\left(\lambda_i, \lambda_j\right) = v_0 \exp\left(-\frac{1}{2}\sum_{n=1}\frac{(\lambda_i^n - \lambda_j^n)^2}{l_n}\right), \tag{20}$$

where $\theta \in \{v_0, l_1, l_2, \dots, l_n\}$, and λ_i^n is nth element of λ_i from data set. Hyperparameters l_n and v_0 represent the length-scale and output-scale, respectively. Consider that a GP prior $\mathcal{G}_{\mathcal{P}}(\boldsymbol{P}|\mu; \mathbf{K})$ is chosen for the constitutive model M, and our experimental data set is $D = [(\lambda_i, P_i)]$, where $P_i = M(\lambda_i) + \epsilon_i$ and $\mathcal{P}(\epsilon|\lambda) = \mathcal{N}(\epsilon, 0; \sigma^2)$; we can write GP prior as

$$\mathcal{P}(\boldsymbol{P}|\theta) = \mathcal{N}\left(\boldsymbol{P}|\mu(\lambda|\theta); \mathbf{K}(\lambda, \lambda|\theta)\right), \tag{21}$$

To fit the hyperparameters, we look for the θ that maximizes the log-likelihood (Lee et al., 2020). Based on Eq. (16) for a Gaussian distribution, log-likelihood can be written as

$$\log \mathcal{P}(\boldsymbol{P}|\lambda, \theta) = -\frac{(\boldsymbol{P} - \mu)^T \mathbf{V}^{-1}(\boldsymbol{P} - \mu)}{2} - \frac{\log \det \mathbf{V}}{2} - \frac{n \log 2\pi}{2}, \quad \text{with}$$

$$\mathbf{V} = \mathbf{K}(\lambda, \lambda|\theta) + \sigma^2 \mathbf{I} \tag{22}$$

Marginal likelihood indicates the quality of the fitting of the model to our training data. To optimize the training and maximize the log-likelihood, the best hyperparameters should be located and used for fitting. In this study, we used L-BFGS method to maximize log-likelihood. Our goal is prediction of function $M(\lambda^*)$ at some test locations λ^*. Now, we can calculate mean and covariance functions at λ and evaluate multivariate Gaussian distribution. So, we can write joint distribution between the training function $M(\lambda) = \boldsymbol{P}$ and the prediction function values $M(\lambda^*) = \boldsymbol{P}^*$. Using Bayes' rule

$$\mathcal{P}\left(\boldsymbol{P}^*|\lambda^*, \boldsymbol{D}\right) = \mathcal{N}\left(\boldsymbol{P}^*|\mu_{\boldsymbol{M}|\boldsymbol{D}}\left(\lambda^*\right); \mathbf{K}_{M|D}(\lambda^*, \lambda^*)\right), \tag{23}$$

where

$$\mu_{\boldsymbol{M}|\boldsymbol{D}}\left(\lambda^*\right) = \mu\left(\lambda^*\right) + \mathbf{K}\left(\lambda^*, \lambda\right)\left(\mathbf{K}(\lambda, \lambda) + \sigma^2 \mathbf{I}\right)^{-1}(\boldsymbol{P} - \mu(\lambda)), \tag{24}$$

(a)   (b)
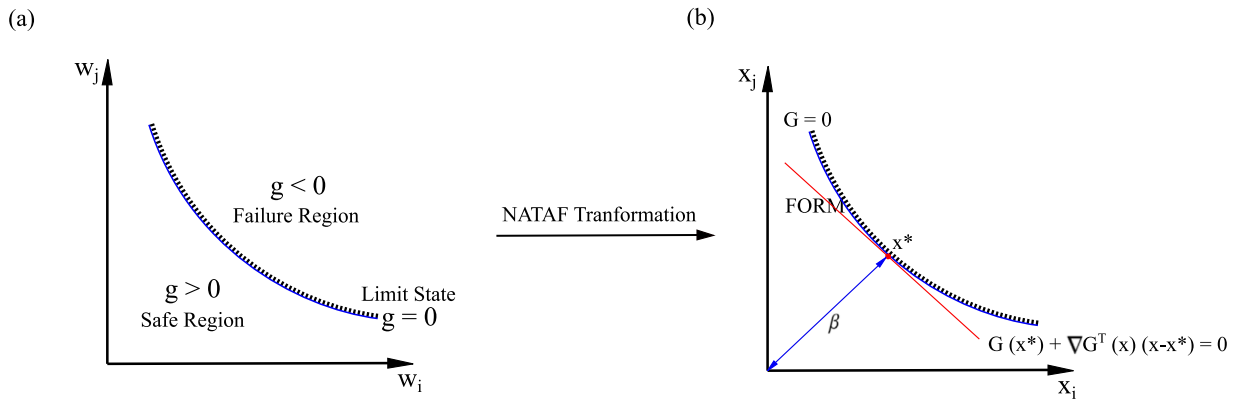

Fig. 1. Concept of β index with respect to LSF in (a) the physical space (b) the standard normal space.

and

$$\mathbf{K}_{M|D}(\lambda^*, \lambda^*) = \mathbf{K}\left(\lambda^*, \lambda^*\right) - \mathbf{K}\left(\lambda^*, \lambda\right)\left(\mathbf{K}(\lambda, \lambda) + \sigma^2 \mathbf{I}\right)^{-1} \mathbf{K}\left(\lambda, \lambda^*\right). \quad (25)$$

where $\mathbf{K}(\lambda, \lambda^*)$ is the cross covariance between λ and λ^*.

4. Probability failure calculation of hyperelastic materials

We explained in the last section how to model uncertainty from different sources into the constitutive models. In this section, we explain how to use a probabilistic model derived from last section as an input in calculation of failure probability.

In failure prediction of hyperelastic materials, uncertainty due to variations in the material matrix (parameter and model uncertainty), compounding (experimental uncertainty), geometry (structural uncertainty), and loading conditions (experimental and interpolation uncertainty) can strongly affect the accuracy of predictions. One main challenge in the development of failure prediction engines is the lack of a certain discrete threshold of failure to describe the phenomena through zero and one events. In practice, samples fail over a wide range of stress or strain amplitudes, which creates a strong margin of error in the deterministic models of failure. To address this problem, probabilistic models are needed to reproduce the probability of failure.

Let us represent the failure stress criteria by σ_U, which can be considered as a deterministic value or a probabilistic distribution (see Fig. 1). Next, by having the probabilistic constitutive behavior of the material $P(\mathbf{W})$, we can derive the failure profile p_f with respect to σ_U using a limit state function (LSF) $g(\mathbf{W})$ as described below.

$$g(\mathbf{W}) = \sigma_U - P(\mathbf{W}), \quad \Rightarrow \quad g(\mathbf{W}) : \begin{cases} > & 0 & \text{Safe region} \\ = & 0 & \text{Limit state} \\ < & 0 & \text{Failure region: } p_f \end{cases}$$

$$(26)$$

where $P(\mathbf{W})$ is a constitutive equation of the variables $W_1, W_2, \ldots, W_n$ which is estimated from the Bayesian surrogate constitutive model procedure which can be derived through aforementioned parametric or non-parametric procedures (see Eq. (3)). The distribution $P(\mathbf{W})$ can be derived based on the experimental data on stress–strain behavior of materials.

NATAF transformation will be used to map the distributions of random constitutive variables, ($\mathbf{W}$), within their standard normal space (for computational purposes Lu et al., 2014). Next, a first-order Taylor expansion at the most probable point is sufficient to locate the maximum failure probability of $g(\mathbf{W})$ (Lebrun and Dutfoy, 2009) (see Fig. 1b). The failure probability P_f integral over the failure region $g < 0$ is written as

$$P_f = \mathcal{P}(g < 0) = \int_{g<0} \ldots \int f\left(W_1, W_2, \ldots, W_n\right) dW_1 \ldots dW_n, \quad (27)$$
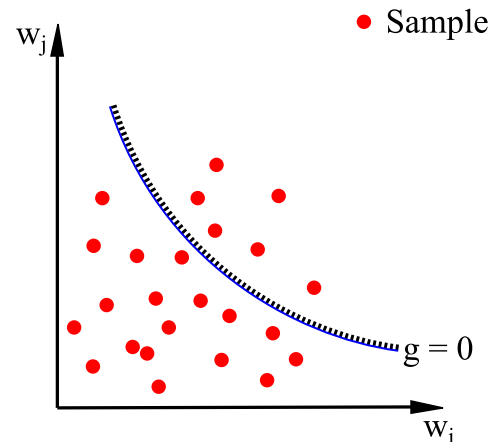

Fig. 2. Monte Carlo simulation.

where f is the probability density function, and n is the size of the input vector $\mathbf{W}$. In Eq. (27), the integral should be taken over p_f where $g < 0$. To simplify the integration, it would be sufficient to rewrite the integration with respect to a normal standard space with $\mu = 0$ and $\sigma = 1$. Accordingly, one can introduce a new limit state function G on a normal standard space which represents the former $g(\mathbf{W})$ over the current space. To convert the problem from current space to the normal standard space, NATAF transformation (Faber, 2009) will be used, which introduce new input parameters x_i based on $\mathbf{W}$ as

$$x_i = \Phi^{-1}\left(f(W_i)\right), \quad (28)$$

where f and Φ^{-1} represents the cumulative distribution functions (CDF) of $\mathbf{W}$ and the inverse CDF of x_i, respectively. Accordingly, P_f is estimated as given below (Lemaire, 2013)

$$P_f = \Phi(-\beta), \quad \beta = \frac{\mu_G}{\sigma_G}, \quad \mu_G \cong G\left(\mu_{x_1}, \mu_{x_2}, \ldots, \mu_{x_n}\right),$$

$$\sigma_G^2 \cong \sum_{i=1}^{n} \sum_{j=1}^{n} \frac{\partial G}{\partial x_i} \frac{\partial G}{\partial x_j} cov\left(x_i, x_j\right), \quad (29)$$

where β is the reliability index, and represents the shortest distance from the origin in standardized normal space to the hyperplane (deterministic) or paraboloid (probabilistic) formed by $G = 0$. β can be calculated by solving an optimization problem. Let us introduce x^* to represent the point along the paraboloid, which has the least distance to the origin, further referred to as the design point. Here, μ_G and σ_G are the mean and standard deviation of the $G(x)$ in the standard normal space. In the FORM analysis, the paraboloid $G(x) = 0$ can be represented by a linear smooth surface which passes through the
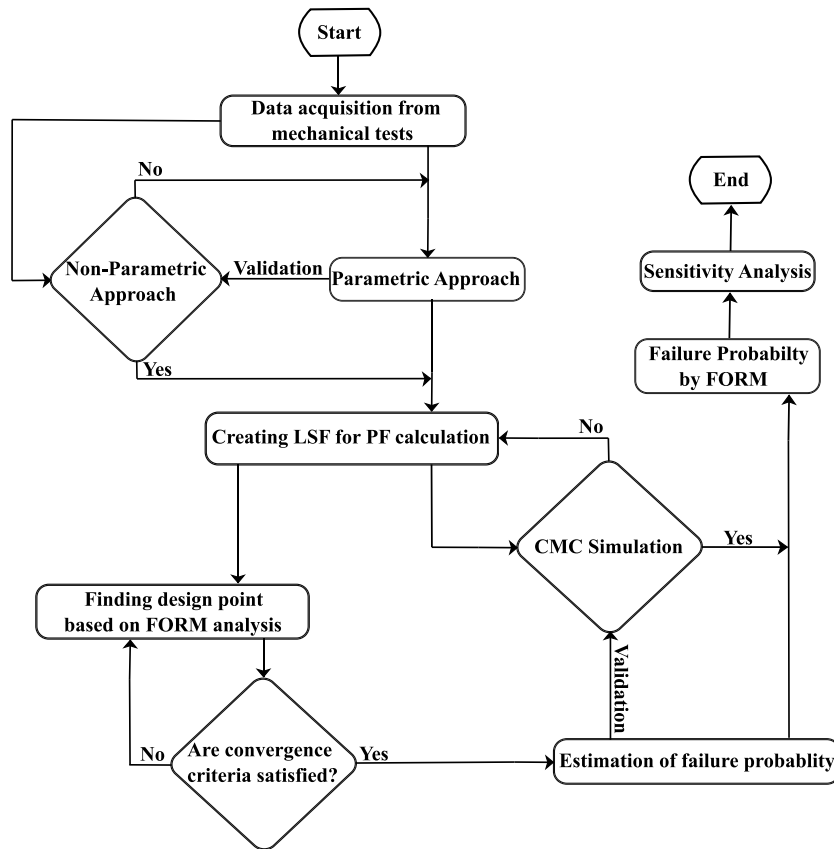
Fig. 3. Flowchart of steps of conducted study.

design point, x^*, designated by position vector $\boldsymbol{x}^*$. Accordingly, we have $G(\boldsymbol{x}) \approx 0$ while $G(\boldsymbol{x}^*) = 0$, and thus the surface can be represented by

$$G(\boldsymbol{x}) = G\left(x^*\right) + \nabla G^T(\boldsymbol{x})\left(\boldsymbol{x} - \boldsymbol{x}^*\right), \qquad \boldsymbol{x}^* = \arg\min\left\{\|\boldsymbol{x}\| \mid G(\boldsymbol{x}) = 0\right\},$$
(30)

where $\beta = \|\boldsymbol{x}^*\|$. The improved Hasofer-Lind-Rackwitz–Fiessler (iHLRF) method is used (Santosh et al., 2006) to find the design point. Furthermore, having an arbitrary point $(\boldsymbol{x}_m)$ as the design point candidate in the iteration m, the new candidate design point $(\boldsymbol{x}_{m+1})$ can be obtained by

$$\boldsymbol{x}_{m+1} = \boldsymbol{x}_m + \delta_m . d_m,$$
(31)

where δ_m, and d_m are the step search and the search direction at the m th iteration, respectively. Here, $\delta_m = a^K$ can be determined by Armijo rule which considers a to be a positive value (usually $a = 0.5$), and k to be an integer that is iteratively increased from zero (Santos et al., 2012). The proper search direction (d_m) and the step search (δ_m) for carrying out the search algorithms to find the design point are presented as follows

$$d_m = \left(\frac{G(\boldsymbol{x}_m)}{\|G(\boldsymbol{x}_m)\|} + \alpha^T \boldsymbol{x}_m\right)\alpha - \boldsymbol{x}_m, \qquad \alpha = \frac{\nabla G(\boldsymbol{x}_m)}{\|\nabla G(\boldsymbol{x}_m)\|}.$$
(32)

A convergence criteria is required to stop the search algorithm for finding $\boldsymbol{x}_m$ which is considered as follows

(1) By assuming $\boldsymbol{x}_m$ to be **almost** on the surface of the limit state function, we have $G(\boldsymbol{x}_m) \approx 0$ which yields

$$\frac{G\left(\boldsymbol{x}_{m+1}\right) - G(x_m)}{G(x_m)} < e_1,$$
(33)

where $e_1 \approx 0.001$ is the convergence parameter that defines the stop criteria.
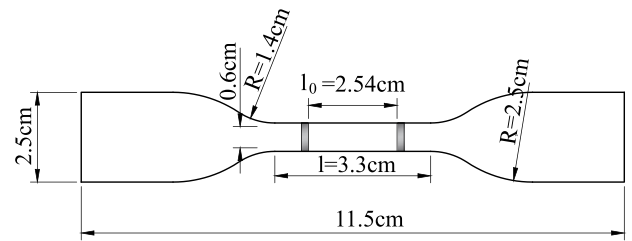

Fig. 4. Detailed sample dimensions.

(2) The surface gradient of the limit state function passes through the coordinate reference point at the last point, which shows that the current point is the closest point to the origin

$$\left|\frac{\boldsymbol{x}_m}{\|\boldsymbol{x}_m\|} - \left(\alpha_m^T \frac{\boldsymbol{x}_m}{\|\boldsymbol{x}_m\|}\right)\alpha_m\right| < e_2,$$
(34)

where e_2 is convergence parameter as a criteria to stop iteration. It is 0.001 based on literature. After finding the design point $(\boldsymbol{x}^*)$, probability of failure is equal to $P_f = \Phi(-\|\boldsymbol{x}^*\|)$.

Crude Monte Carlo (CMC) Simulation is used to provide benchmark for validating the predictions obtained by FORM. CMC simulation is also used concurrently to estimate the limit state probabilities. The results show the accuracy of the first-order approximation of LSF. CMC is a popular method among the methods of sampling which generates random numbers for random variables $\boldsymbol{W}$, based on their distribution. Each time a random vector is generated, $g(\boldsymbol{W})$ will be validated and consequently, we assume sample failure if $g(\boldsymbol{W}) < 0$ (see Fig. 2). Integral of failure probability can be written as

$$P_f = \mathcal{P}(g < 0) = \int_{g<0} \dots \int f(\boldsymbol{W})\, d\boldsymbol{W} = \int_{-\infty}^{+\infty} \dots \int_{-\infty}^{+\infty} I(\boldsymbol{W})\, f(\boldsymbol{W})\, d\boldsymbol{W}$$
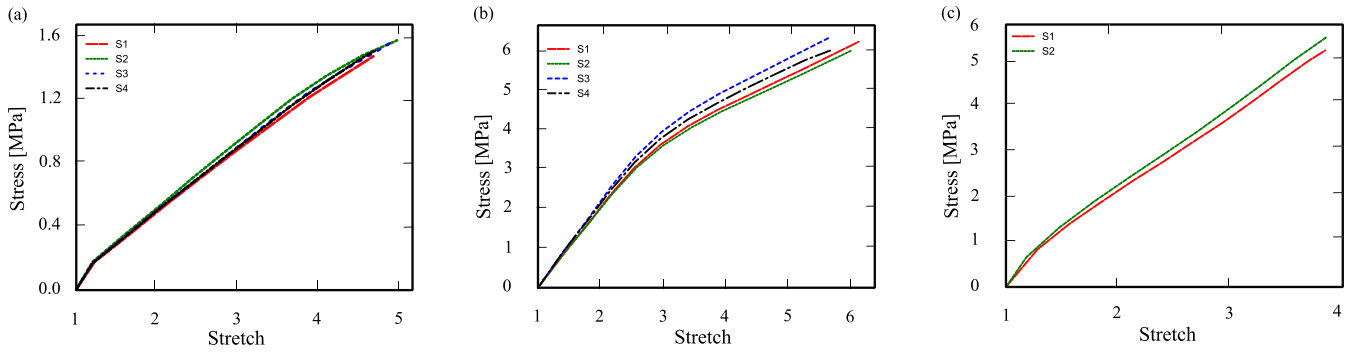
Fig. 5. Stretch–stress results of mechanical tests for (a) Silicone, (b) Polyurethane (c)Styrene-butadiene rubber.
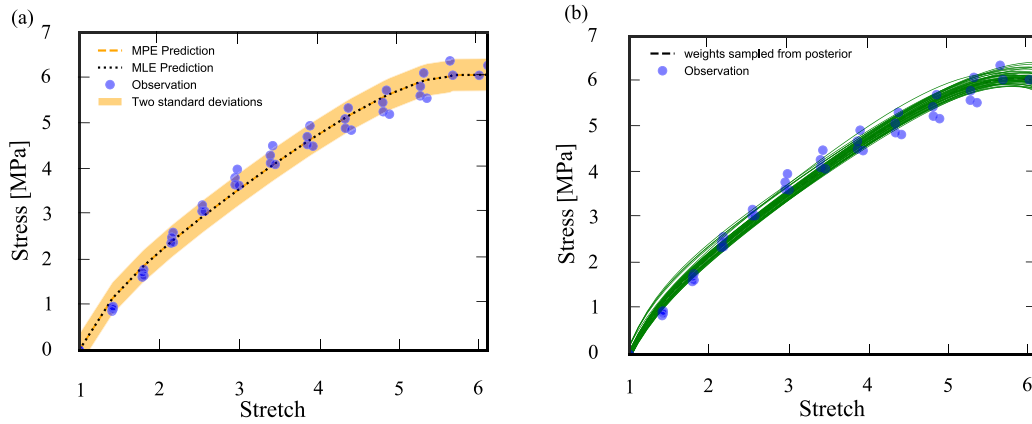

Fig. 6. Model calibration of Carroll model for Polyurethane (a) prediction (b) plausible models.
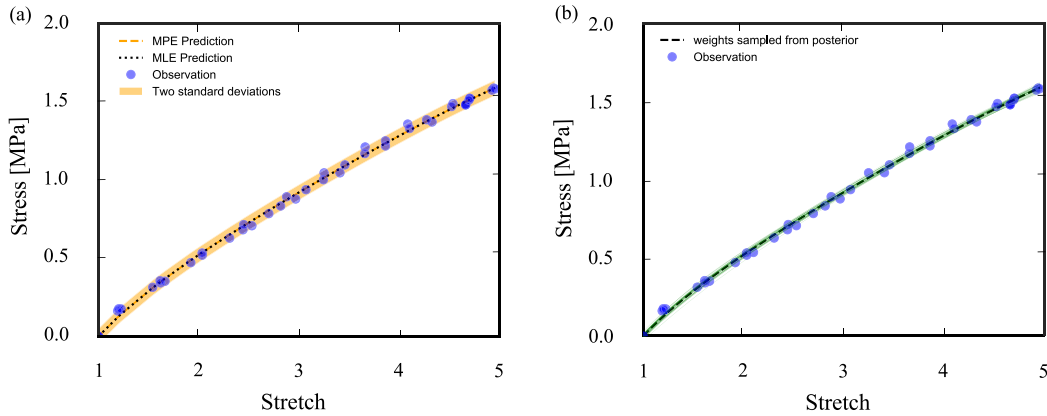

Fig. 7. Model calibration of Carroll model for Silicone (a) prediction (b) plausible models.

$$= \frac{1}{N} \sum_{i=1}^{N} I\left(W_i\right), \tag{35}$$

where $N = \frac{1}{\delta_{P_f}^2}\left(\frac{1-P_f}{P_f}\right)$ is the number of simulation, and $\delta_{P_f} = 0.05$ is a common value in the literature (Lemaire, 2013; Xiukai et al., 2020).

Note that Monte Carlo simulations constitute an integration method which, with respect to numerical integration, represents an economical means of choosing only some points by chance in the integration domain instead of systematically scanning in all directions. The value of the integration is thus deduced from the mathematical expectations of the sampling. On the other hand, FORM is a method which includes an integration method by estimation of LSF with Taylor expansion. The reason that we represent and compare these methods is that we want to show with CMC that first-order estimation of LSF in FORM is correct

or not. So, if their results are in a good agreement, it means that the estimation is correct.

For understanding the procedure of this research, the below flowchart shows the steps of this study in summary (see Fig. 3).

Sensitivity Analysis

Importance vector, γ, is used as a computational tool to determine the relative influence of the parameters in the failure probability function in the reliability analysis. Since now we can approximate the limit state function around the design point $G(x) = \|\nabla G(x^*)\|\left(\beta - \alpha^T x\right)$, variance of LSF, namely $var(G)$, can be written as follows

$$var(G) = \nabla G^T \Sigma_{xx} \nabla G = \left(- \|\nabla G\| \alpha\right)^T \left(- \|\nabla G\| \alpha\right)$$
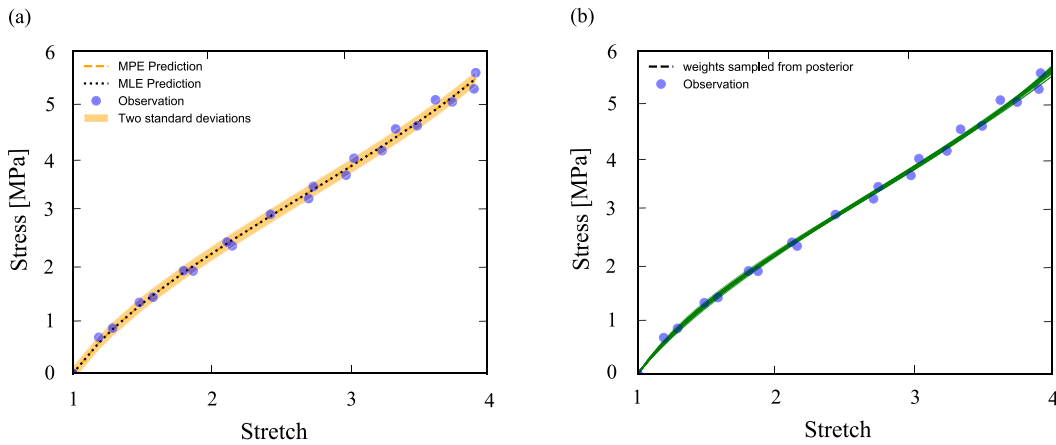$$= \|\nabla G\|^2 \left(\alpha_1^2 + \alpha_2^2 + \cdots + \alpha_n^2\right), \tag{36}$$

Fig. 8. Model calibration of Carroll model for Styrene-butadiene rubber (a) prediction (b) plausible models.
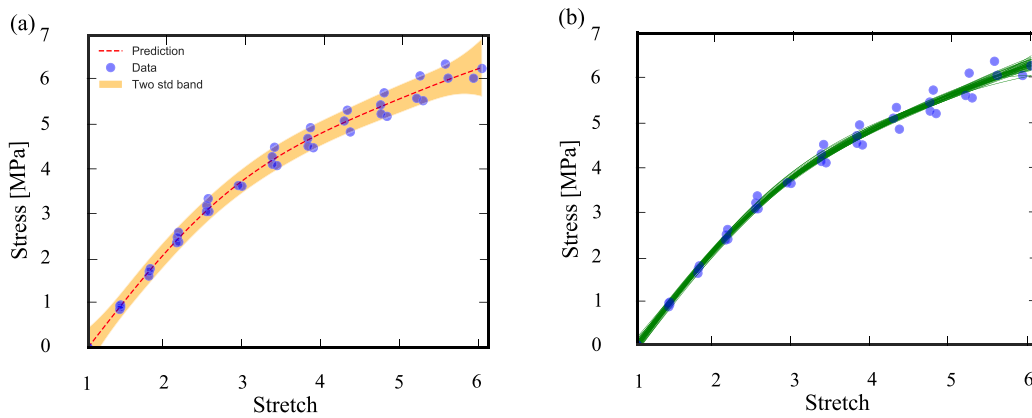

Fig. 9. GP model for Polyurethane (a) prediction (b) plausible models.

where Σ_{xx} is the covariance matrix. In Eq. (36), we define the contribution of each random variable in the variance of the limit state function through α_i^2 with higher values of $|\alpha_i|$ representing larger influence of their associated random variables. If $\alpha_i > 0$, the random variable is called the load variable, and is called the resistance variable otherwise when $\alpha_i < 0$. So, whenever the FORM analysis is carried out to derive γ, one can determine the significance of random variables, which has the greatest interference in the probability of failure. To consider the correlation between the variables, the importance vector γ is defined as follows

$$\gamma = \frac{\alpha j_{x^*,w^*} \mathbf{D}}{\|\alpha j_{x^*,w^*} \mathbf{D}\|}, \tag{37}$$

where $\mathbf{j}_{x,w} = \mathbf{DL}$. Here, $\mathbf{D}$ is the derivation matrix in $\sigma = \mathbf{DRD}$ where $\mathbf{R}$ is the correlation coefficient matrix, and $\mathbf{L}$ is derived as the Cholesky factor of the upper triangle of $\mathbf{R}$, namely $\mathbf{L} = chol(\mathbf{R})$.

5. Results

5.1. Experimental tests

A uni-axial test is implemented for three materials, silicon, polyurethane black, and Styrene-butadiene rubber. Four specimens were used to characterize each failure point used in the experimental data. Our tests were mostly focused on uniaxial tensile tests performed on Dumbbell specimen with specifications given in ASTM D412-Die C and shown in Fig. 4.

Table 1
Statistical characteristics of Carroll model for Polyurethane.

Parameters	Statistical distribution	Mean value	Standard deviation	Coefficient of variation
W1	Normal	0.61025	0.01555	0.0255
W2	Normal	−5.4944e−7	0.9059e−7	0.1648
W3	Normal	0.09649	0.23623	2.4481

Mechanical test. Quasi-static tensile tests were conducted on a uniaxial universal Testing Machine (*TestResources* 311 Series Frame). Samples were clamped between two grips and stretched at the rate of 50 mm/min at room conditions to minimize the visco-elastic effects(i.e. $22 \pm 2 \,°C, 50 \pm 3\% RH$). Measurement is conducted using an external extensometer to avoid clamp slippage. In Fig. 5, stretch–stress curves are depicted for all samples and as illustrated, the samples failure were very close to each other in small deformation. As deformation increases, the evolution of defects in the samples leads to uncertainty in the material's response.

Parametric stochastic constitutive model. Model calibration is conducted based on Bayesian regression to demonstrate UQ of Carroll model with respect to the behavior of three elastomeric compounds, silicon, polyurethane, and styrene-butadiene rubber (SBR). MLE and MAP of the Carroll model were derived for three materials, while several plausible models of MAP are plotted in Figs. 6, 7, and 8 for polyurethane and Silicone, respectively. Similarly, Table 1, 2, and 3 show the stochastic parameters for Silicone, Polyurethane, and Styrene-butadiene rubber.

Non-parametric stochastic constitutive model. To see the non-parametric model's performance, a GP analysis is conducted on these data sets
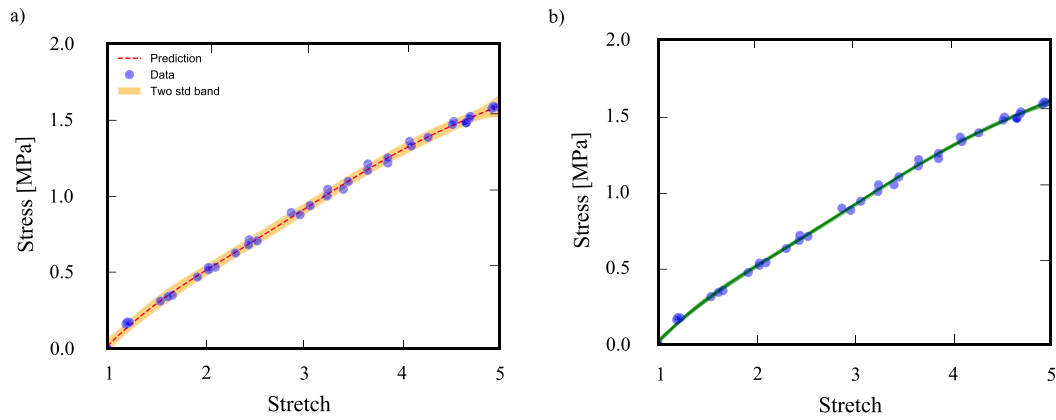
Fig. 10. GP model for Silicone (a) prediction (b) plausible models.
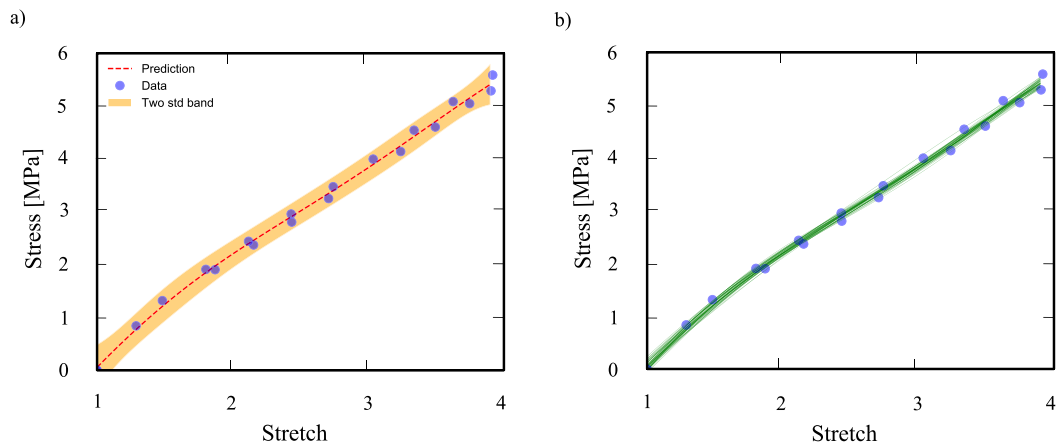

Fig. 11. GP model for Styrene-butadiene rubber (a) prediction (b) plausible models.

Table 2
Statistical characteristics of Carroll model for Silicone.

Parameters	Statistical distribution	Mean value	Standard deviation	Coefficient of variation
W1	Normal	0.173568	0.002315	0.013341
W2	Normal	−8.43e−8	3.492e−8	0.414199
W3	Normal	−0.206981	0.028986	0.140046

Table 3
Statistical characteristics of Carroll model for Styrene-butadiene rubber.

Parameters	Statistical distribution	Mean value	Standard deviation	Coefficient of variation
W1	Normal	0.671017	0.01242	0.01851
W2	Normal	3.5265e−6	1.567e−6	0.4443
W3	Normal	−0.3385	0.03127	0.09237

to find hyper-parameters of the kernel in GP. We maximized log-likelihood based on L-BFGS method for two experimental data sets. Figs. 9, 10, 11 show the results for Polyurethane, Silicone, and Styrene-butadiene rubber respectively. Besides, several plausible models are plotted based on obtained hyperparameters. Data is more scatter in larger deformation due to the breakage of some samples and cumulative errors with stretch increasing. Note that we employed homoscedastic noise in the case study and this is the reason which initial stretch of curves have uncertainty. To make it zero, we can use heteroscedastic sparse Gaussian processes which Bessa et al. (2019) and Zhang et al. (2019) employed to design a metamaterial and quantify the uncertainty.

Probability of failure. For failure analysis, the first step is creating the limit state function $g(\boldsymbol{W})$. Based on the previously derived stochastic constitutive model, $g(\boldsymbol{W})$ can be written as

$$g(\boldsymbol{W}) = \sigma_U - \left(2W_1 + 8W_2 \left(2\lambda^{-1} + \lambda^2 \right)^3 + W_3 \left(1 + 2\lambda^3 \right)^{-\frac{1}{2}} \right) \left(\lambda - \lambda^{-2} \right),$$

(38)

where we consider $\lambda = 5.861$ for Polyurethane predictions, $\lambda = 4.815$ for Silicone, and $\lambda = 3.91$ for Styrene-butadiene which are the mean of stretch in experimental datasets. Note that the selection of stretch for failure probability calculation depends on how much we stretch the material.

Failure distribution pattern for Polyurethane, Silicone, Styrene-butadiene can be best represented by $\sigma_U = \mathcal{N}(6.19, 0.16)$, $\sigma_U = \mathcal{N}(5.9, 0.237)$, and $\sigma_U = \mathcal{N}(5.45, 0.145)$ respectively. Those distributions were derived based on the data of four samples at failure points (i.e., a distribution analysis on failure points of four samples in each case). Table 4 shows the results of FORM analysis and CMC for Polyurethane, Silicone, Styrene-butadiene rubber. Also, Figs. 12, 13, and 14 Show the details of CMC simulation and distribution of $g(\boldsymbol{W})$ analysis for Polyurethane, Silicone, Styrene-butadiene rubber, respectively.

Accordingly, the derived failure probability exhibits the probability of material failure at any specific stretch values. To show the importance of the random variables in failure probability, a sensitivity analysis has also been conducted, and the results for Polyurethane, Silicone, and Styrene-butadiene are shown in Fig. 15.
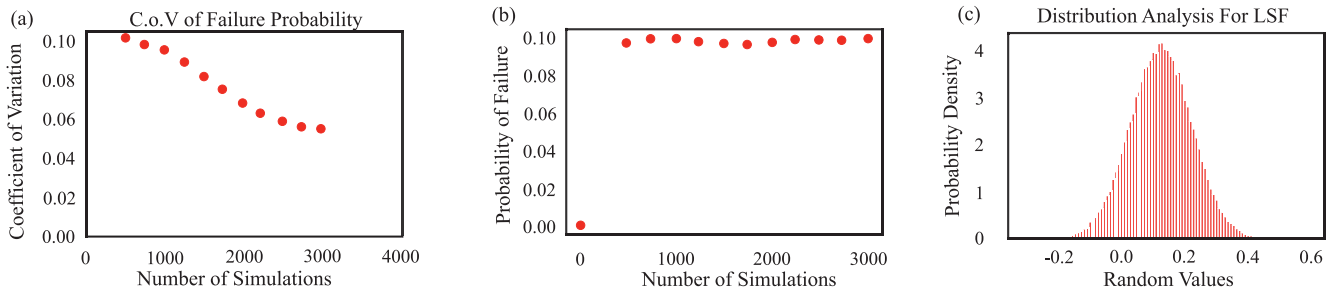
Fig. 12. Polyurethane: (a) coefficient of variation for failure probability respect to number of simulation (b) probability of failure respect to number of simulation (c) LSF distribution analysis.
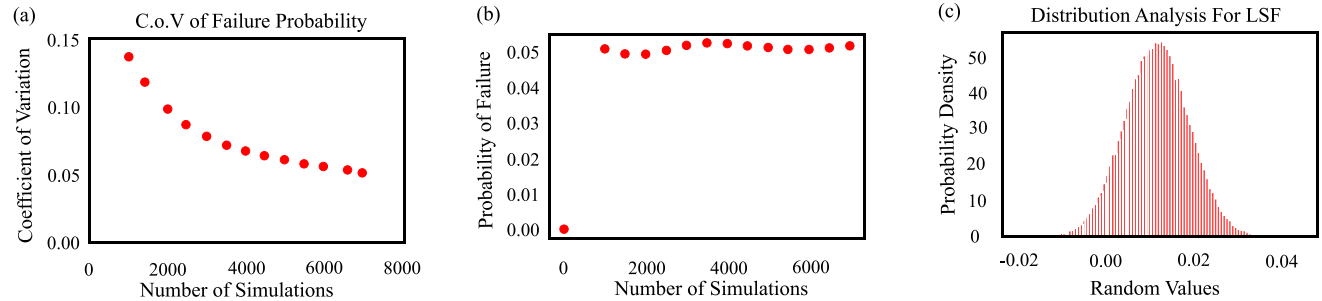

Fig. 13. Silicone: (a) coefficient of variation for failure probability respect to number of simulation (b) probability of failure respect to number of simulation (c) LSF distribution analysis.
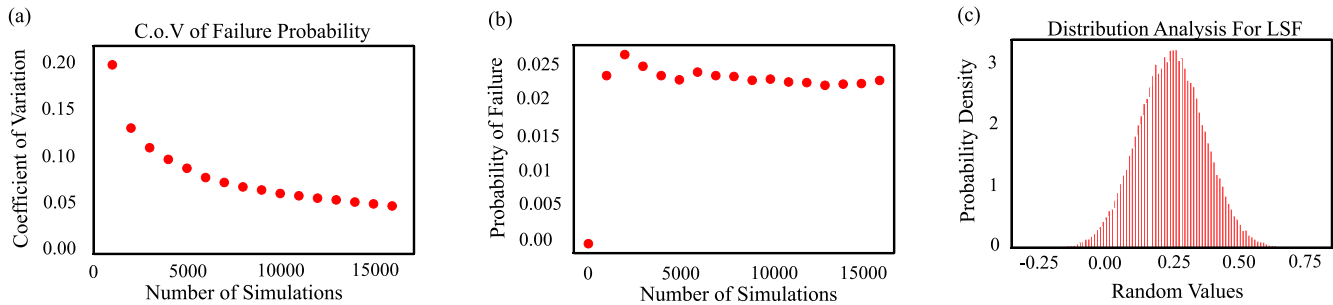

Fig. 14. Styrene-butadiene: (a) coefficient of variation for failure probability respect to number of simulation (b) probability of failure respect to number of simulation (c) LSF distribution analysis.
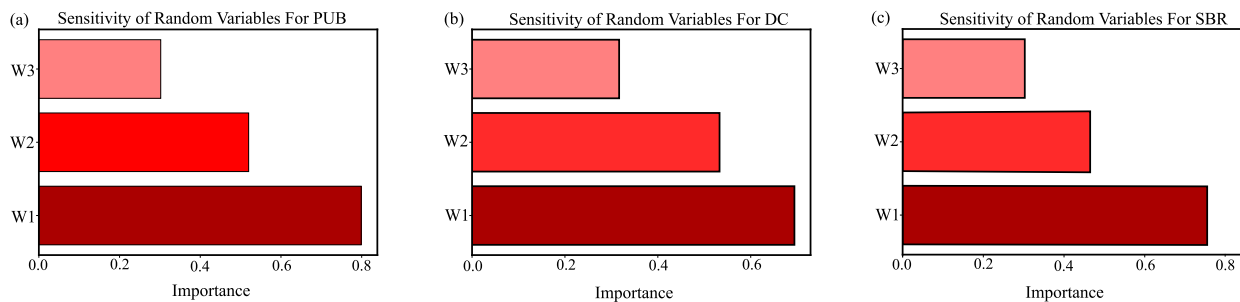

Fig. 15. Importance analysis (a) for Polyurethane (b) for Silicone (c) for Styrene-butadiene.

6. Concluding remarks

This paper developed a Bayesian surrogate constitutive model to estimate failure probability of elastomers. First, a comprehensive uncertainty analysis was conducted and validated at multiple stage, including a parametric Bayesian inference on Caroll model which was calibrated based on two methods (MAP and MLE), a non-parametric Gaussian process which is based on squared exponential kernel. Both models were trained and validated with respect to two sets of our experiments

on silicon- and polyurethane-based elastomers to demonstrate their capabilities in explaining uncertainty propagation. Next, For these data sets, failure probability analysis was performed using the First Order Reliability Method (FORM) by constructing a limit state function based on the stochastic constitutive model at the failure point. Crude Monte Carlo (CMC) simulation was used concurrently to estimate the limit state probabilities in order to determine the validity of adopting FORM. Finally, the importance of Carroll model parameters in predicting failure probability was demonstrated using sensitivity analysis.

Table 4
Probability of failure for Polyurethane, Silicone, Styrene-butadiene based on FORM and CMC.

Method	PUB[a]		DC[b]		SBR[c]	
	FORM	CMC	FORM	CMC	FORM	CMC
P_f (%)	10.185	9.725	5.577	5.671	2.2903	2.3235
β	1.2710	1.2973	1.5912	1.5829	1.9971	1.9910

[a]Polyurethane.

[b]Silicone.

[c]Styrene-butadiene.

The developed framework is generic and can be implemented on any combination of data and constitutive model.

CRediT authorship contribution statement

Aref Ghaderi: Conceptualization, Methodology, Software, Validation, Formal analysis, Investigation, Data curation, Writing – original draft, Visualization. **Vahid Morovati:** Conceptualization, Methodology, Investigation, Writing – original draft. **Roozbeh Dargazany:** Conceptualization, Methodology, Resources, Writing – review & editing, Supervision, Project administration, Funding acquisition.

Declaration of competing interest

The authors declare that they have no known competing financial interests or personal relationships that could have appeared to influence the work reported in this paper.

Acknowledgment

Appendix. Continuum mechanics

Consider that $\mathbf{X}$ and $\mathbf{x}$ are the reference and current coordinates of an element under deformation $\mathbf{x} = D(\mathbf{X})$ in a body which D is a mapping function and $\mathbf{F} = \frac{\partial \mathbf{x}}{\partial \mathbf{X}}$ known as deformation gradient. We can define right Cauchy-green deformation tensor as $\mathbf{C} = \mathbf{F}^T \mathbf{F}$. λ_k and λ_k^2, $k = 1, 2, 3$, are eigenvalues of $\mathbf{F}$ and $\mathbf{C}$, respectively. The principal invariant of $\mathbf{C}$ mentioned as

$$\mathbf{I}_1(\mathbf{C}) = tr(\mathbf{C}), \qquad \mathbf{I}_2(\mathbf{C}) = \frac{1}{2}\left((\mathbf{I}_1(\mathbf{C}))^2 - tr(\mathbf{C}^2)\right),$$

$$\mathbf{I}_3(\mathbf{C}) = \det(\mathbf{C}). \tag{A.1}$$

The strain energy function can be defined as

$$\Psi = \Psi(\mathbf{C}) = \Psi\left(\mathbf{I}_1, \mathbf{I}_2, \mathbf{I}_3\right). \tag{A.2}$$

First Piola–Kirchhoff stress tensor $\mathbf{P}$ can be written as

$$\mathbf{P} = \frac{\partial \Psi}{\partial \mathbf{F}} - p\mathbf{F}^{-T}. \tag{A.3}$$

For incompressible elastomers, $\det \mathbf{F} = 1$ and p is a Lagrange multiplier that arises from the assumption of incompressibility.

References

Adler, R.J., 2010. The Geometry of Random Fields. SIAM.

Arruda, E.M., Boyce, M.C., 1993. A three-dimensional constitutive model for the large stretch behavior of rubber elastic materials.

Berger, J.O., Bernardo, J.M., 1992. On the development of the reference prior method. Bayesian Stat. 4 (4), 35–60.

Berger, J.O., Pericchi, L.R., Ghosh, J., Samanta, T., De Santis, F., Berger, J., Pericchi, L., 2001. Objective Bayesian Methods for Model Selection: Introduction and Comparison. In: Lecture Notes-Monograph Series, pp. 135–207.

Berk, R.H., 1966. Limiting behavior of posterior distributions when the model is incorrect. Ann. Math. Stat. 51–58.

Bessa, M.A., Bostanabad, R., Liu, Z., Hu, A., Apley, D.W., Brinson, C., Chen, W., Liu, W.K., 2017. A framework for data-driven analysis of materials under uncertainty: Countering the curse of dimensionality. Comput. Methods Appl. Mech. Engrg. 320, 633–667.

Bessa, M.A., Glowacki, P., Houlder, M., 2019. Bayesian machine learning in metamaterial design: Fragile becomes supercompressible. Adv. Mater. 31 (48), 1904845.

Bostanabad, R., Liang, B., van Beek, A., Gao, J., Liu, W.K., Cao, J., Zeng, D., Su, X., Xu, H., Li, Y., et al., 2020. 11.1 background and literature review. In: Uncertainty Quantification in Multiscale Materials Modeling. Woodhead Publishing Limited, p. 355.

Box, G.E., Tiao, G.C., 2011. Bayesian Inference in Statistical Analysis, Vol. 40. John Wiley & Sons.

Brewick, P.T., Teferra, K., 2018. Uncertainty quantification for constitutive model calibration of brain tissue. J. Mech. Behav. Biomed. Mater. 85, 237–255.

Burr, T.L., 2004. Bayesian Inference: Parameter Estimation and Decisions. Taylor & Francis.

Cao, L., Liu, J., Xie, L., Jiang, C., Bi, R., Non-probabilistic polygonal convex set model for structural uncertainty quantification. Appl. Math. Model. 89, 504–518,

Carroll, M., 2011. A strain energy function for vulcanized rubbers. J. Elasticity 103 (2), 173–187.

Chen, T., Martin, E., 2009. Bayesian linear regression and variable selection for spectroscopic calibration. Anal. Chim. Acta 631 (1), 13–21.

Dal, H., Açıkgöz, K., Badienia, Y., 2021. On the performance of isotropic hyperelastic constitutive models for rubber-like materials: A state of the art review. Appl. Mech. Rev. 73 (2), 020802.

Dimitrov, N., Bitsche, R., Blasques, J., 2017. Spatial reliability analysis of a wind turbine blade cross section subjected to multi-axial extreme loading. Struct. Saf. 66, 27–37.

Faber, M.H., 2009. Basics of Structural Reliability. Swiss Federal Institute of Technology ETH, Zürich, Switzerland.

Fitt, D., Wyatt, H., Woolley, T.E., Mihai, L.A., 2019. Uncertainty quantification of elastic material responses: testing, stochastic calibration and Bayesian model selection. Mech. Soft Mater. 1 (1), 13.

Fuhg, J.N., Böhm, C., Bouklas, N., Fau, A., Wriggers, P., Marino, M., 2021a. Model-data-driven constitutive responses: application to a multiscale computational framework. arXiv preprint arXiv:2104.02650.

Fuhg, J.N., Marino, M., Bouklas, N., 2021b. Local approximate Gaussian process regression for data-driven constitutive laws: Development and comparison with neural networks. arXiv preprint arXiv:2105.04554.

Ghaderi, A., Morovati, V., Dargazany, R., 2020. A physics-informed assembly of feed-forward neural network engines to predict inelasticity in cross-linked polymers. arXiv preprint arXiv:2007.03067.

Ghanipour, A., Ghavanloo, E., Fazelzadeh, S., Pouresmaeeli, S., 2018. Uncertainty propagation in the buckling behavior of few-layer graphene sheets. Microsyst. Technol. 24 (2), 1167–1177.

Honarmandi, P., 2019. Materials Design Under Bayesian Uncertainty Quantification (Ph.D. thesis).

Jaynes, E.T., 2003. Probability Theory: The Logic of Science. Cambridge University Press.

Kamiński, M., Lauke, B., 2018. Probabilistic and stochastic aspects of rubber hyperelasticity. Meccanica 53 (9), 2363–2378.

Khashaba, U., Aljinaidi, A., Hamed, M., 2017. Fatigue and reliability analysis of nano-modified scarf adhesive joints in carbon fiber composites. Composites B 120, 103–117.

Lebrun, R., Dutfoy, A., 2009. Do Rosenblatt and Nataf isoprobabilistic transformations really differ? Probab. Eng. Mech. 24 (4), 577–584.

Lee, T., Bilionis, I., Tepole, A.B., 2020. Propagation of uncertainty in the mechanical and biological response of growing tissues using multi-fidelity Gaussian process regression. Comput. Methods Appl. Mech. Engrg. 359, 112724.

Lemaire, M., 2013. Structural Reliability. John Wiley & Sons.

Liao, Z., Hossain, M., Yao, X., 2020. Ecoflex polymer of different shore hardnesses: experimental investigations and constitutive modelling. Mechanics of Materials 144, 103366.

Liao, Z., Yang, J., Hossain, M., Chagnon, G., Jing, L., Yao, X., 2021. On the stress recovery behaviour of Ecoflex silicone rubbers. Int. J. Mech. Sci. 106624.

Liu, Z., Bessa, M., Liu, W.K., 2016. Self-consistent clustering analysis: an efficient multiscale scheme for inelastic heterogeneous materials. Comput. Methods Appl. Mech. Engrg. 306, 319–341.

Lu, D., Song, P., Liu, Y., Yu, X., 2014. An extended first order reliability method based on generalized Nataf transformation. In: Deodatis, G., Ellingwood, B.R., Frangopol, D.M. (Eds.), Safety, Reliability, Risk and Life-Cycle Performance of Structures and Infrastructures. CRC Press, pp. 1177–1184.

Madireddy, S., Sista, B., Vemaganti, K., 2015. A Bayesian approach to selecting hyperelastic constitutive models of soft tissue. Comput. Methods Appl. Mech. Engrg. 291, 102–122.

Mihai, L.A., Woolley, T.E., Goriely, A., 2018. Stochastic isotropic hyperelastic materials: constitutive calibration and model selection. Proc. R. Soc. A 474 (2211), 20170858.

Mishra, M., Keshavarzzadeh, V., Noshadravan, A., 2019. Reliability-based lifecycle management for corroding pipelines. Struct. Saf. 76, 1–14.

Mooney, M., 1940. A theory of large elastic deformation. J. Appl. Phys. 11 (9), 582–592.

Ogden, R.W., 1972. Large deformation isotropic elasticity–on the correlation of theory and experiment for incompressible rubberlike solids. Proc. R. Soc. Lond. Ser. A Math. Phys. Eng. Sci. 326 (1567), 565–584.

Orta, L., Bartlett, F., 2015. Reliability analysis of concrete deck overlays. Struct. Saf. 56, 30–38.

Planas, R., Oune, N., Bostanabad, R., 2021. Evolutionary Gaussian processes. J. Mech. Des. 143 (11), 111703.

Pouresmaeeli, S., Fazelzadeh, S., Ghavanloo, E., Marzocca, P., 2018. Uncertainty propagation in vibrational characteristics of functionally graded carbon nanotube-reinforced composite shell panels. Int. J. Mech. Sci. 149, 549–558.

Rasmussen, C.E., 2003. Gaussian processes in machine learning. In: Summer School on Machine Learning. Springer, pp. 63–71.

Rivlin, R., 1948. Large elastic deformations of isotropic materials. I. Fundamental concepts. Phil. Trans. R. Soc. A 240 (822), 459–490.

Robert, C., 2007. The Bayesian Choice: From Decision-Theoretic Foundations to Computational Implementation. Springer Science & Business Media.

Rocchetta, R., Broggi, M., Patelli, E., 2018. Do we have enough data? Robust reliability via uncertainty quantification. Appl. Math. Model. 54, 710–721.

Santos, S., Matioli, L., Beck, A., 2012. New optimization algorithms for structural reliability analysis. Comput. Model. Eng. Sci. (CMES) 83 (1), 23–55.

Santosh, T., Saraf, R., Ghosh, A., Kushwaha, H., 2006. Optimum step length selection rule in modified HL–RF method for structural reliability. Int. J. Press. Vessels Pip. 83 (10), 742–748.

Steinmann, P., Hossain, M., Possart, G., 2012. Hyperelastic models for rubber-like materials: consistent tangent operators and suitability for Treloar's data. Arch. Appl. Mech. 82 (9), 1183–1217.

Teferra, K., Brewick, P.T., 2019. A Bayesian model calibration framework to evaluate brain tissue characterization experiments. Comput. Methods Appl. Mech. Engrg. 357, 112604.

Tipping, M.E., 2001. Sparse Bayesian learning and the relevance vector machine. J. Mach. Learn. Res. 1 (Jun), 211–244.

Vila, J.-P., Wagner, V., Neveu, P., 2000. Bayesian nonlinear model selection and neural networks: A conjugate prior approach. IEEE Trans. Neural Netw. 11 (2), 265–278.

Xiukai, Y., Zhenxuan, Z., Baoqiang, Z., 2020. Augmented line sampling for approximation of failure probability function in reliability-based analysis. Appl. Math. Model. 80, 895–910.

Yang, Q., Meng, S., Jin, H., Xie, W., Zhang, X., 2019. Multi-fidelity uncertainty quantification method with application to nonlinear structural response analysis. Appl. Math. Model. 75, 853–864.

Zhang, W., Bostanabad, R., Liang, B., Su, X., Zeng, D., Bessa, M.A., Wang, Y., Chen, W., Cao, J., 2019. A numerical Bayesian-calibrated characterization method for multiscale prepreg preforming simulations with tension-shear coupling. Compos. Sci. Technol. 170, 15–24.